

Understanding the Temperature Dependence of the Seebeck Coefficient from First-Principles Band Structure Calculations for Organic Thermoelectric Materials

Ran Liu, Yufei Ge, Dong Wang & Zhigang Shuai*

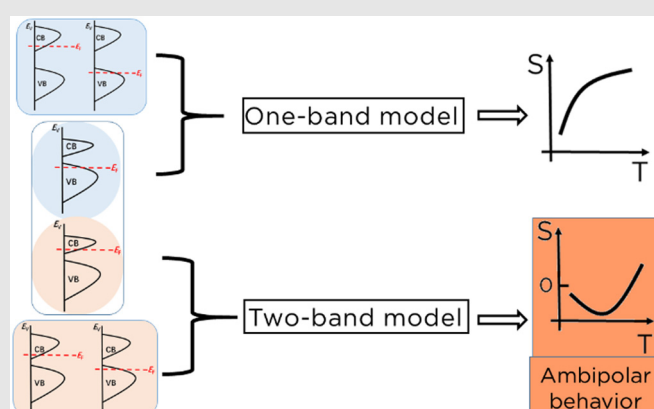
MOE Key Laboratory of Organic OptoElectronics and Molecular Engineering, Department of Chemistry, Tsinghua University, Beijing 100084

*Corresponding author: zgshuai@tsinghua.edu.cn

Cite this: CCS Chem. 2021, 3, 1477–1483

The Seebeck effect measures the electric potential built up in materials under a temperature gradient. For organic thermoelectric materials, the Seebeck coefficient shows more complicated temperature dependence than conventional systems, with both monotonic increases and nonmonotonic behavior, that is, first increasing and then decreasing. The mechanism behind the phenomenon is intriguing. Through first-principles calculations coupled with the Boltzmann transport equation, we demonstrate typical trends of the Seebeck coefficient with respect to temperature through band structure analysis. The bandgap and bandwidths of the valence band and conduction band jointly determine the effectiveness of thermal activation. Ineffective or effective thermal activation leads to a one- or a two-band transport behavior, respectively. Under the thermal-activation mechanism, Seebeck coefficient shows monotonic temperature dependence in a one-band model but nonmonotonic relationship in a two-band model. In particular, in the

two-band model, Seebeck coefficient might show an ambipolar behavior, that is, its sign changes at high temperature.



Keywords: organic thermoelectric materials, Seebeck coefficient, band structure calculation, ambipolar thermoelectric transport, Boltzmann transport equation

Introduction

Organic thermoelectric materials (OTEs) have aroused great interests and have been rapidly developed in recent years.^{1–7} Compared with inorganic thermoelectric materials, OTEs show lower thermal conductivity, high cost-effectiveness, and low toxicity. Doping conducting polymers are very promising OTEs. Both *p*- and *n*-type polymers have rapidly developed with figure of merit *zT* increases from 10^{-3} to 0.4.^{3,8} The effects of oxidation,⁹ pressure,¹⁰ and temperature have been studied. There have been many experimental results^{11,12} demonstrating the temperature dependence of Seebeck coefficient, *S*. For example, for the polymer blends poly(3,4-ethylenedioxithiophene):poly(styrenesulfonate)/polypyrrole (PEDOT: PSS/PPy), Li et al.¹³ showed that *S* monotonically increases with *T*. For doped poly(2,5-bis(3-tetradecylthiophen-2-yl)thieno[3,2-*b*]thiophene) (PBTTT) films with thermal annealing beforehand and potassium-doped poly(nickel-ethylenetetrathiolate) [poly(Ni-ett)], Zhang et al.¹⁴ and Sun et al.¹⁵ showed that when *T* increases, *S* first increases, then levels off, and finally decreases at higher *T*. It must be mentioned that thermopower measurements for organic conductors have been performed for a long time. For example, in 1986, Zhu et al.¹⁶ measured the Seebeck coefficient for β -(Bis(ethylenedithio)tetrathiafulvalene)₂Brl₂ (β -(BEDT-TTF)₂Brl₂) and surprisingly, Seebeck coefficients even change sign from negative to positive with increasing temperature, demonstrating an exotic ambipolar transport behavior. Such behavior has never been explained. Recently, Liu et al.¹⁷ have shown significant boosting effects of polaron bands in *K*-doped poly(Ni-ett), and the abnormal temperature dependence can be explained by polaron formation.

We note that a number of complicating factors (e.g., structural deformation, dominant dopant, and polaron formation) were included in previous work to understand the relationship between *S* and *T*. In this work, we intend to avoid the complexation of doping, and we illustrate the abnormal Seebeck coefficient versus temperature behavior can be understood from electronic structures, as will be shown through different band structures with variant bandwidths and band gaps. We believe such a basic understanding can be extended to more complicated situation with only analysis for density of states (DOS).

Applying first-principles computations based on density functional theory under the deformation potential (DP) approximation^{18–20} in combination with the Boltzmann transport equation,^{21,22} we try to understand the relationship between *S* and *T* from the intrinsic band structure. In fact, from the textbook knowledge, for metallic behavior,²³ *S* increases with *T* ($S = -\frac{\pi^2 k_B}{3} e K_B T \frac{d \ln \sigma(e)}{de}|_{e=e_F}$, see Supporting Information Figure S1) and for semiconductors,²⁴ doped carriers can be thermally activated to the conduction or valence band (VB), leading to a $1/T$ dependence ($S = \frac{C}{T} + D$,

see Supporting Information Figure S2). It is expected that when the bandgap is large, only the VB or conduction band (CB) participates in the transport, that is, one-band model is applicable. When the bandgap is small enough, both VB and CB might participate in the transport together at high temperature, with their contributions determined by their bandwidths. If the bandwidths of VB and CB are widely different, the transport model depends on the location of the Fermi level. Specifically, when the Fermi level is in the broad band, only the broadband participates in transport. While when the Fermi level is in the narrow band, both VB and CB will participate in transport together, that is, a two-band model is applicable. If the bandwidths of VB and CB are of small difference, VB and CB will participate in transport together for the Fermi level inside VB or CB. Here, we demonstrate that using both one- and two-band models, the complicated temperature dependence of Seebeck coefficients found in PPy and poly(Ni-tetrathiofulvalene-tetrathiolate) [poly(Ni-ttftt)]²⁵ can be explained.

Computational Methods

Electronic structure calculations

The polymer backbones lie along the *X* axis, and the vacuums layers along the *Y* and *Z* axes are large enough to ensure the isolated “ideal” polymer chains. The different functionals have been adopted for PPy and poly(Ni-ttftt). The projector augmented wave method with Perdew–Burke–Ernzerhof (PBE)²⁶ for PPy and local-density approximation (LDA) + *U* (*U* = 6.04 eV)²⁷

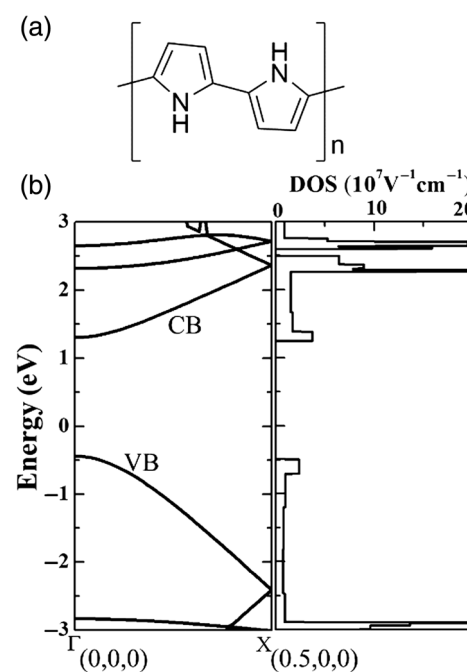


Figure 1 | (a) Chemical structure and (b) band structure and DOS of PPy.

Table 1 | The Elastic Constant, C_{ii} , Electron DP Constant, $E_{1(e)}$, and Hole DP Constant, $E_{1(h)}$

Polymer	C_{ii} (10^{-8} J m^{-1})	$E_{1(e)}$ (eV)	$E_{1(h)}$ (eV)
PPy	8.766	5.57	4.86
Poly(Ni-ttftt)	7.379	4.39	1.85

for poly(Ni-ttftt) were adopted for the optimization of the lattice parameters of X axis and ionic positions and their electron structure calculations in the Vienna Ab initio Simulation Package.²⁸

Thermoelectric transport coefficients calculations

In the Boltzmann transport theory,²⁹ the electrical conductivity, σ , and Seebeck coefficient, S , are expressed as:

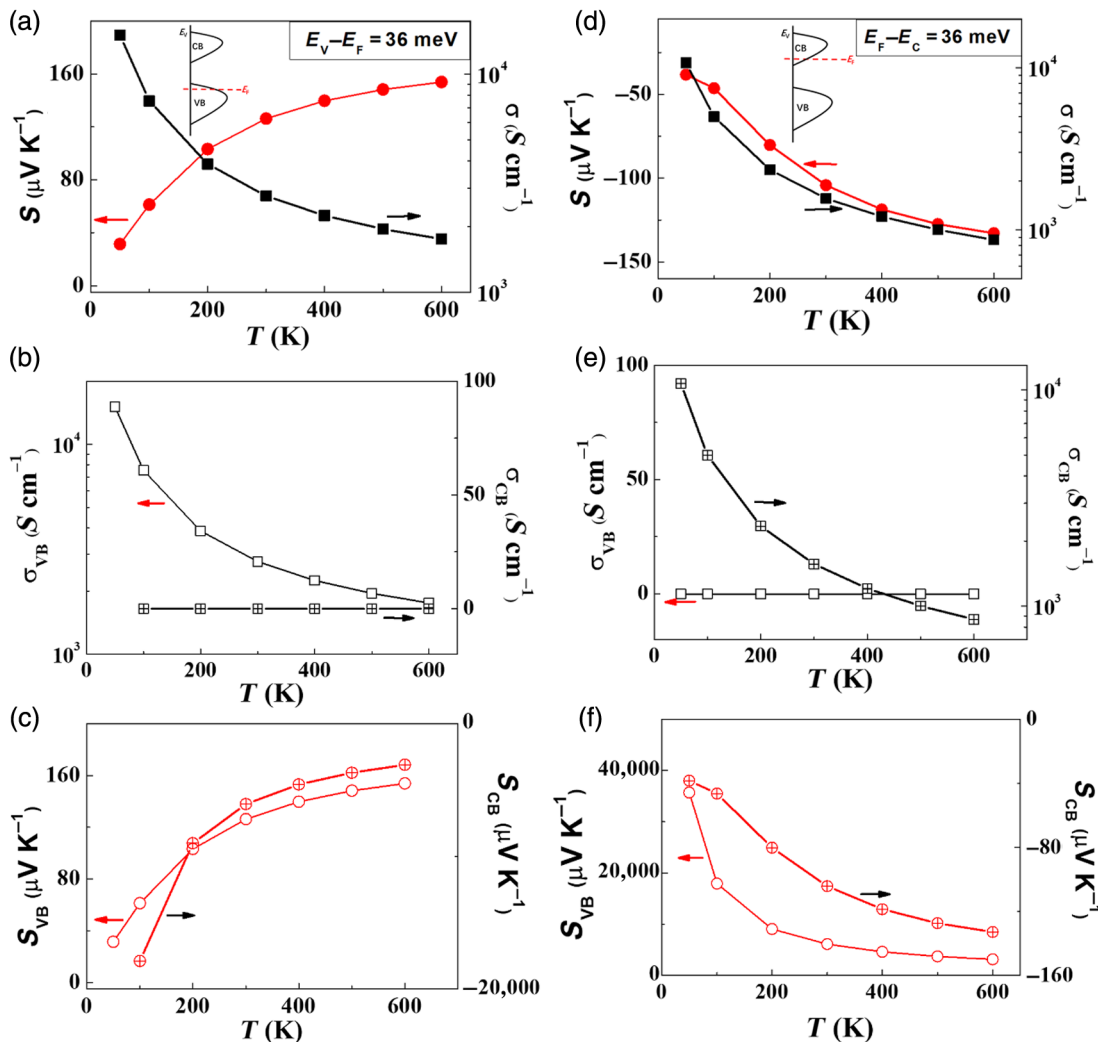
$$\sigma = e^2 \sum_k \left(-\frac{\partial f_0(\epsilon_k)}{\partial \epsilon_k} \right) v_k v_k \tau_k \quad (1)$$

$$S = \frac{e}{\sigma T} \sum_k \left(-\frac{\partial f_0(\epsilon_k)}{\partial \epsilon_k} \right) (\epsilon_k - \epsilon_F) v_k v_k \tau_k \quad (2)$$

where $f_0(\epsilon_k) = 1/[\exp((\epsilon_k - \epsilon_F)/k_B T) + 1]$ is the Fermi-Dirac distribution function; $\partial f_0(\epsilon_k)/\partial \epsilon_k$ is nonzero only when ϵ_k locates within $k_B T$ near the Fermi level. ϵ_k is the band energy at k -point; ϵ_F is the Fermi energy; $v_k = (1/\hbar) \nabla_k \epsilon_k$ is the group velocity; τ_k is the relaxation time due to scattering with phonons and/or disorders/impurities.

If both VB and CB contribute to transport, the effective total S can be expressed as³⁰:

$$S = \frac{S_{VB}\sigma_{VB} + S_{CB}\sigma_{CB}}{\sigma_{VB} + \sigma_{CB}} \quad (3)$$

**Figure 2 |** Total S and σ , σ_{VB} and σ_{CB} , and S_{VB} and S_{CB} of p- and n-type doping of PPy with 1.74 eV bandgap change with T . (a) to (c) are for p-doping. (d) to (f) are for n-doping. The location of Fermi level (E_F) in the insert indicates the doping concentration and type.

Here, S_{VB} and S_{CB} are the Seebeck coefficients for VB and CB, respectively, and σ_{VB} and σ_{CB} are the corresponding electrical conductivities. It is worth noting that S is positive for hole and negative for electron transport in doped semiconductors.

Relaxation time calculations

Under the DP approximation with longitudinal phonon scattering, the relaxation time can be expressed as²¹: $1/\tau_k = (2\pi/\hbar) \sum_{k'} |M(k,k')|^2 \delta(\epsilon_k - \epsilon_{k'}) (1 - \cos \theta)$, where θ is the scattering angle between k and k' , and $|M(k,k')|^2$ is the scattering matrix element, which takes the form $|M(k,k')|^2 = k_B T E_1^2 / C_{ii}$, where E_1 is DP constant and C_{ii} is elastic constant, in the long wave limit $k \rightarrow 0$. The thermoelectric (TE) transport coefficients were calculated based on the BoltzTrap program.³¹ Last, the relaxation time was obtained from first-principles calculations.^{21,32}

Results and Discussion

First of all, the geometric structure of PPy was optimized, and its band structure was calculated (Figures 1a and 1b). The electron-phonon coupling is quantitatively described by DP constant and elastic constant in DP theory, and all DP constants and elastic constants are summarized in Table 1.

PPy can be easily *p*-doped.^{33–36} So, we placed the Fermi level inside VB, and the transport behavior in VB belongs to metallic behavior. The positive S monotonically increases with increasing T in Figure 2a, compliant with metallic behavior (Figure 2c, hollow line). This phenomenon can be explained by eq. 3. In this case, eq. 3 is simplified to $S \approx S_{VB}$ because of $\sigma_{VB}/\sigma \gg \sigma_{CB}/\sigma$ ($\sigma = \sigma_{VB} + \sigma_{CB}$, Figure 2b) even at $T = 600$ K. These can be understood from two aspects: (1) the term of $d\sigma_0(\epsilon_k)/d\epsilon_k$ in CB is vanishingly small because of the large bandgap (1.74 eV) (Figure 1b). (2) The large bandgap also makes thermal activation from VB to CB impossible. So, there is hardly any electrons in CB even at high T . Therefore, VB is the only band participating in transport. This causality also applies to the situation of Fermi level inside CB (Figures 2d–2f). To summarize, the TE properties of PPy with the 1.74 eV bandgap belong to one-band transport behavior. For either *p*- or *n*-type doping, $|S|$ monotonically increases with increasing T .

To reveal the role of bandgap in the TE properties, we studied metal coordinated polymer poly(Ni-ttftt) (Figures 3a and 3b). The calculated bandgap is 0.12 eV, consistent with the previous result.²⁵ Since the nickel-coordinated polymers can be *n*-doped in the experiment,^{15,25} we first placed the Fermi level inside CB. We find that the Seebeck coefficient has an ambipolar behavior, namely, at relatively low-temperature range, negative S nonmonotonically changes with increasing T , and

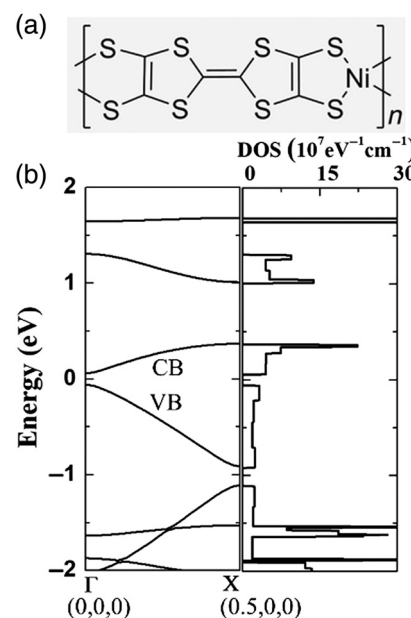


Figure 3 | (a) Chemical structure and (b) band structure and DOS of poly(Ni-ttftt).

at very high T , the sign of S changes, shown in Figure 4a. Such ambipolar behavior can be explained again by eq. 3. At very low T , eq. 3 is simplified to $S \approx S_{CB}$ because of $\sigma_{VB}/\sigma \ll \sigma_{CB}/\sigma$ (Figure 4b), so only CB participates in the transport. As T increases, σ_{VB}/σ and σ_{CB}/σ get close. So, the transport behavior is determined by CB (metallic model behavior, Figure 4c, cross line) and VB (semiconductor model behavior, Figure 4c, hollow line) together. As T continues to rise, σ_{VB}/σ and σ_{CB}/σ get closer, even $\sigma_{VB}/\sigma \approx \sigma_{CB}/\sigma$, and $S_{VB} > S_{CB}$, according to eq. 3, the sign of S becomes positive, leading to an exotic ambipolar behavior. The large σ_{VB} at high T is attributed to thermal activation, and the thermal activation is attributed to a small bandgap. Overall, under the thermal-activation mechanism, the two-band model determines that S non-monotonically changes with increasing T , that is, first increases at low T , then decreases at high T , and its sign changes at much higher T .

Then we placed the Fermi level inside the VB of poly(Ni-ttftt) to look at *p*-type doping. Figure 4d shows that positive S monotonically increases with increasing T . Figures 4e and 4f show that the impact of $\sigma_{VB}/\sigma \gg \sigma_{CB}/\sigma$ is much greater than $S_{CB} > S_{VB}$, which means that eq. 3 will be simplified to $S \approx S_{VB}$. So, VB is the only band participating in the transport, and the temperature dependence of S is consistent with the VB transport behavior (Figure 4f, hollow line).

For poly(Ni-ttftt), the trends of S with increasing T of *p*- and *n*-type doping are completely different. This can be attributed to the difference in bandwidths of VB and CB. The bandwidths of VB and CB are 0.86 and 0.31 eV, respectively, that is, relatively big difference. The wider

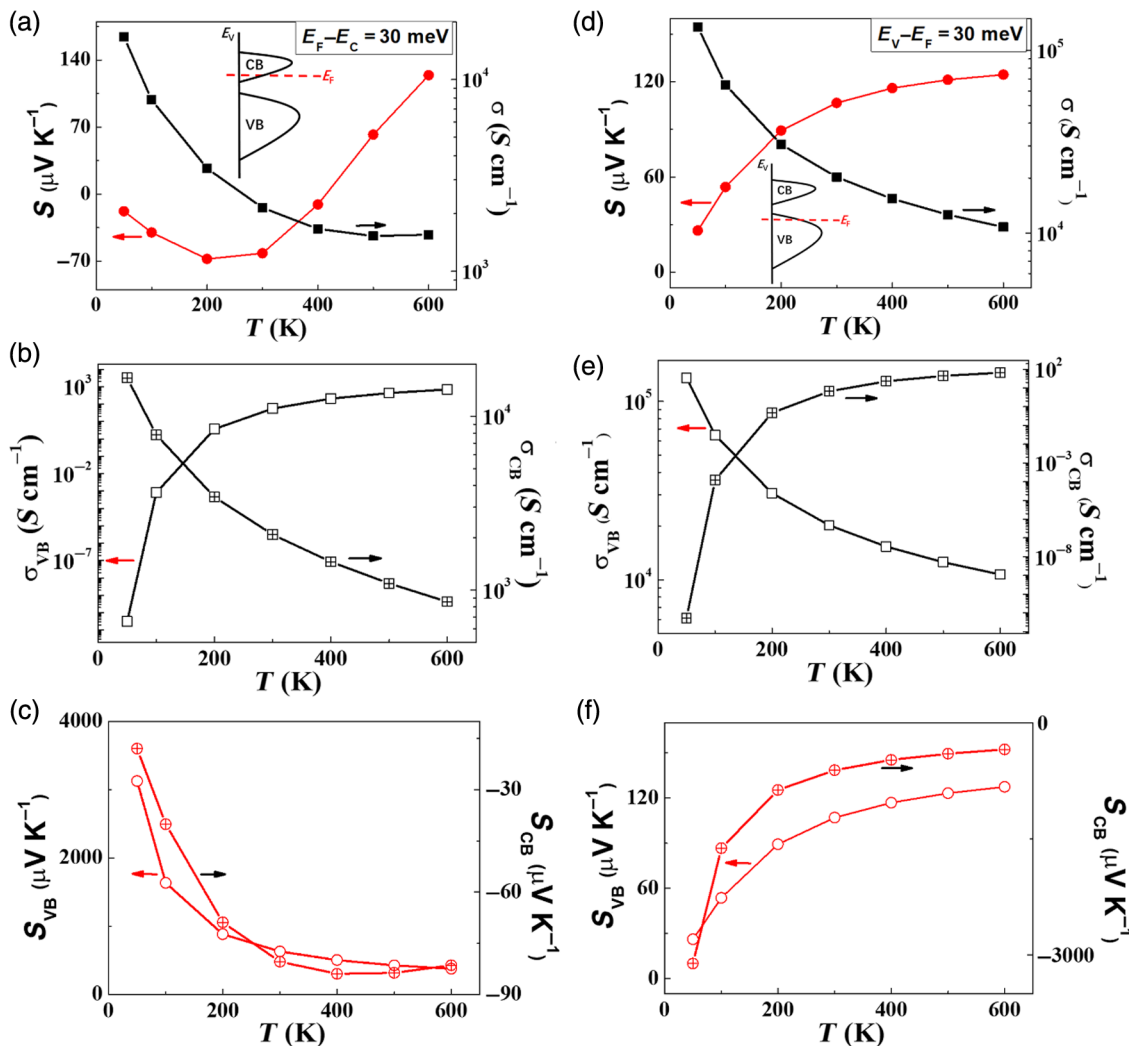


Figure 4 | Total S and σ , σ_{VB} and σ_{CB} , and S_{VB} and S_{CB} of n- and p-type doping of poly(Ni-ttftt) with 0.12 eV bandgap change with T . (a) to (c) are for n-doping. (d) to (f) are for p-doping.

the bandwidth, the smaller the effective mass, or the better for transport. So, at high T , given the fixed small bandgap, the relationship between σ_{VB}/σ and σ_{CB}/σ is quite different, that is, $\sigma_{VB}/\sigma \sim \sigma_{CB}/\sigma$ for n-type doping and $\sigma_{VB}/\sigma \gg \sigma_{CB}/\sigma$ for p-type doping. According to eq. 3, n- and p-type doping of poly(Ni-ttftt) correspond to two- and one-band transport model, respectively, which can explain the nonmonotonic and monotonic relationship between S and T . In particular, at $T > 400$ K, S of n-type doping becomes positive, that is, ambipolar behavior. It is most interesting to mention here that in 1986, Zhu et al.¹⁶ have already observed the very first ambipolar thermopower for $(\text{BEDT-TTF})_2\text{BrI}_2$, a donor-acceptor-type organic conductor, for which the Seebeck coefficient looked quite similar to Figure 4a. Currently, we are investigating in more details for such exotic behavior.

Based on the above results, we conclude that, given a small bandgap, if the bandwidths of VB and CB are of small difference, VB and CB will participate in transport

together for both n- and p-type doping. To obtain a small bandgap, the scissor operator in Boltztrap program was adopted to PPy, with small differences of bandwidths of CB and VB. Results show that (1) as the bandgap gets smaller, the relationship between S and T becomes non-monotonic for Fermi level inside VB or CB (see Supporting Information Figure S4), (2) when the bandgap is small enough, σ_{VB}/σ and σ_{CB}/σ are close at high T , which means the transport model is a two-band model for Fermi level inside VB or CB (see Supporting Information Figure S5) and S nonmonotonically changes with increasing T . In short, when the bandgap is small enough, the bandwidth effect of VB and CB should be considered to determine the transport model.

Conclusions

OTEs have been found to demonstrate vastly different temperature dependent of Seebeck coefficient, indicating

rich physics behind the complicated thermoelectric transport behavior. Through first-principles computational study, we revealed the relationship between band structure (bandgap and bandwidth) of OTEs and the temperature dependence of Seebeck coefficient for some model polymer systems. For the case of large bandgap, when thermal activation can be excluded, only one band (VB or CB) contributes to transport. If the bandgap is small enough, the bandwidth effect of VB and CB should be considered to determine the transport model. Specifically, (1) if the bandwidths are of big difference, the transport model depends on the doping type. When Fermi level is placed in the narrow band, the thermally activated electrical conductivity from the broadband should be considered at high T . So, both VB and CB participate (two-band model) in transport together. When Fermi level is located in the broadband, the thermally activated electrical conductivity of narrow band can be ignored even at very high T . So, only the broadband participates in transport. (2) If the bandwidths are of small difference, VB and CB will participate in transport together for the Fermi level inside VB or CB. Under the thermal activation mechanism, the one-band model means that S monotonically increases with increasing T , and the two-band model means that S nonmonotonically changes with increasing T , and, at very high T , S has ambipolar behavior. In the experiment, the monotonic temperature dependence of S had been found for PF_6^- -doped PPy, and iodine-doped polyacetylene³⁷ and the ambipolar behavior have been measured in $(\text{BEDT-TTF})_2\text{BrI}_2$,¹⁶ tetrathiafulvalene[bis-1,3-dithio-2-thione-4,5-dithiolato-nickelate]₂ (TTF[Ni(dmit)₂]₂),³⁸ and polyaniline (PANI)/Bi₂S₃.³⁹ From our theoretical studies here, we can attribute these behaviors to be one- and two-band model, respectively. So, the band structure can well explain the relationship between S and increasing T . We believe better understanding is the starting point for material design with targeted properties. For example, experimentalists may choose the proper T that the material can exhibit bigger PF by the trend of S with T , because Seebeck coefficient has the major contribution into the material PF, $\text{PF} = S^2\sigma$. Our results can be generalized to amorphous phases. One can predict the trends of S with T based on the DOS for both crystals and amorphous phases based on our analysis. Furthermore, by considering more types of scattering interaction, for example, ion scattering and optical phonon scattering, the relationship between TE properties and temperature will be more accurately understood. We need to stress that band picture is the simplest picture, but the physics behind this phenomenon could be employed to understand more complicated situations, such as in a case of doping-induced localized DOS.

Supporting Information

Supporting Information is available and includes additional figures and results.

DOI: 10.31635/ccschem.021.202100813

CCS Chem. 2021, 3, 1477–1483

Conflict of Interest

There is no conflict of interest to report.

Funding Information

This work is supported by the National Natural Science Foundation of China through the project “Science Center for Luminescence from Molecular Aggregates” (SCELMA; grant no. 201788102) and the Ministry of Science and Technology of China through the National Key R&D Plan (grant no. 2017YFA0204501).

Acknowledgments

Z.S. is deeply indebted to Professor Daoben Zhu for the stimulating discussion, especially for his introduction to the fascinating field of organic thermoelectric, in addition to bringing the attention of his pioneering work of ref 16.

References

- Bubnova, O.; Crispin, X. Towards Polymer-Based Organic Thermoelectric Generators. *Energy Environ. Sci.* **2012**, 5, 9345–9362.
- Kim, G. H.; Shao, L.; Zhang, K.; Pipe, K. P. Engineered Doping of Organic Semiconductors for Enhanced Thermoelectric Efficiency. *Nat. Mater.* **2013**, 12, 719–723.
- Russ, B.; Glaudell, A.; Urban, J. J.; Chabiny, M. L.; Segalman, R. A. Organic Thermoelectric Materials for Energy Harvesting and Temperature Control. *Nat. Rev. Mater.* **2016**, 1, 1–14.
- Sun, Y.; Sheng, P.; Di, C.; Jiao, F.; Xu, W.; Qiu, D.; Zhu, D. Organic Thermoelectric Materials and Devices Based on p- and n-Type Poly(Metal 1,1,2,2-Ethenetetrathiolate)s. *Adv. Mater.* **2012**, 24, 932–937.
- Zhang, F.; Zang, Y.; Huang, D.; Di, C. A.; Zhu, D. Flexible and Self-Powered Temperature-Pressure Dual-Parameter Sensors Using Microstructure-Frame-Supported Organic Thermoelectric Materials. *Nat. Commun.* **2015**, 6, 8356.
- Zhang, Q.; Sun, Y. M.; Xu, W.; Zhu, D. Organic Thermoelectric Materials: Emerging Green Energy Materials Converting Heat to Electricity Directly and Efficiently. *Adv. Mater.* **2014**, 26, 6829–6851.
- Wang, L.; Jiang, Q.; Zhao, D.; Zhang, Q.; Jia, Y.; Gu, C.; Hu, D.; Ma, Y. Triazine and Porphyrin-Based Cross-Linked Conjugated Polymers: Protonation-Assisted Dissolution and Thermoelectric Properties. *CCS Chem.* **2020**, 2, 2688–2695.
- He, J.; Tritt, T. M. Advances in Thermoelectric Materials Research: Looking Back and Moving Forward. *Science* **2017**, 357, 1369.
- Liu, S.; Deng, H.; Zhao, Y.; Ren, S.; Fu, Q. The Optimization of Thermoelectric Properties in a PEDOT:PSS Thin Film through Post-Treatment. *RSC Adv.* **2015**, 5, 1910–1917.
- Alsaleh, N. M.; Shoko, E.; Arsalan, M.; Schwingenschlögl, U. Thermoelectric Materials under Pressure. *Phys. Status Solidi RRL* **2018**, 12, 1800083.

11. Huang, D.; Yao, H.; Cui, Y.; Zou, Y.; Zhang, F.; Wang, C.; Shen, H.; Jin, W.; Zhu, J.; Diao, Y.; Xu, W.; Di, C. A.; Zhu, D. Conjugated-Backbone Effect of Organic Small Molecules for n-Type Thermoelectric Materials with ZT over 0.2. *J. Am. Chem. Soc.* **2017**, *139*, 13013–13023.
12. Sheng, P.; Sun, Y.; Jiao, F.; Liu, C.; Xu, W.; Zhu, D. Optimization of the Thermoelectric Properties of Poly [Cu_x(Cu-Ethylenetetrathiolate)]. *Synth. Met.* **2014**, *188*, 111–115.
13. Li, J.; Du, Y.; Jia, R.; Xu, J.; Shen, S. Z. Thermoelectric Properties of Flexible PEDOT:PSS/Polypyrrole/Paper Nano-composite Films. *Materials (Basel)* **2017**, *10*, 780.
14. Zhang, Q.; Sun, Y.; Jiao, F.; Zhang, J.; Xu, W.; Zhu, D. Effects of Structural Order in the Pristine State on the Thermoelectric Power-Factor of Doped PBTTT Films. *Synth. Met.* **2012**, *162*, 788–793.
15. Sun, Y.; Qiu, L.; Tang, L.; Geng, H.; Wang, H.; Zhang, F.; Huang, D.; Xu, W.; Yue, P.; Guan, Y. S.; Jiao, F.; Sun, Y.; Tang, D.; Di, C. A.; Yi, Y.; Zhu, D. Flexible n-Type High-Performance Thermoelectric Thin Films of Poly(Nickel-Ethylenetetrathiolate) Prepared by an Electrochemical Method. *Adv. Mater.* **2016**, *28*, 3351–3358.
16. Zhu, D.; Wang, P.; Wan, M.; Yu, Z.; Zhu, N. Synthesis, Structure and Electrical Properties of the Two-Dimensional Organic Conductor, (BEDT-TTF)₂Brl₂. *Physica* **1986**, *143B*, 281–284.
17. Liu, Y.; Shi, W.; Zhao, T.; Wang, D.; Shuai, Z. Boosting the Seebeck Coefficient for Organic Coordination Polymers: Role of Doping-Induced Polaron Band Formation. *J. Phys. Chem. Lett.* **2019**, *10*, 2493–2499.
18. Bardeen, J.; Shockley, W. Deformation Potentials and Mobilities in Non-Polar Crystals. *Phys. Rev.* **1950**, *80*, 72–80.
19. Wang, D.; Tang, L.; Long, M.; Shuai, Z. First-Principles Investigation of Organic Semiconductors for Thermoelectric Applications. *J. Chem. Phys.* **2009**, *131*, 224704.
20. Long, M.-Q.; Tang, L.; Wang, D.; Wang, L.; Shuai, Z. Theoretical Predictions of Size-Dependent Carrier Mobility and Polarity in Graphene. *J. Am. Chem. Soc.* **2009**, *131*, 17728–17729.
21. Wang, D.; Shi, W.; Chen, J.; Xi, J.; Shuai, Z. Modeling Thermoelectric Transport in Organic Materials. *Phys. Chem. Chem. Phys.* **2012**, *14*, 16505–16520.
22. Chen, J.; Wang, D.; Shuai, Z. First-Principles Predictions of Thermoelectric Figure of Merit for Organic Materials: Deformation Potential Approximation. *J. Chem. Theory Comput.* **2012**, *8*, 3338–3347.
23. Fritzsche, H. A General Expression for the Thermoelectric Power. *Solid State Commun.* **1971**, *9*, 1813–1815.
24. Rowe, D. M. *Thermoelectrics Handbook: Macro to Nano*; CRC Press: Boca Raton, FL, **2006**.
25. Shi, W.; Wu, G.; Yong, X.; Deng, T.; Wang, J. S.; Zheng, J. C.; Xu, J.; Sullivan, M. B.; Yang, S. W. Orbital-Engineering-Based Screening of π-Conjugated d⁸ Transition-Metal Coordination Polymers for High-Performance n-Type Thermoelectric Applications. *ACS Appl. Mater. Interfaces* **2018**, *10*, 35306–35315.
26. Perdew, J.; Burke, K.; Ernzerhof, M. Generalized Gradient Approximation Made Simple. *Phys. Rev. Lett.* **1996**, *77*, 3865–3868.
27. Zhou, F.; Cococcioni, M.; Marianetti, C. A.; Morgan, D.; Ceder, G. First-Principles Prediction of Redox Potentials in Transition-Metal Compounds With LDA+U. *Phys. Rev. B* **2004**, *70*, 235121.
28. Kresse, G.; Furthmüller, J. Efficient Iterative Schemes for Ab Initio Total-Energy Calculations Using a Plane-Wave Basis Set. *Phys. Rev. B* **1996**, *54*, 11169–11186.
29. Ziman, J. M. *Principles of the Theory of Solid*; Cambridge University Press: Cambridge, MA, **1971**.
30. Emin, D. *Polarons*; Cambridge University Press: New York, **2013**.
31. Madsen, G. K. H.; Singh, D. Boltztrap. A Code for Calculating Band-Structure Dependent Quantities. *Comput. Phys. Commun.* **2006**, *175*, 67–71.
32. Shuai, Z.; Wang, D.; Peng, Q.; Geng, H. Computational Evaluation of Optoelectronic Properties for Organic/Carbon Materials. *Acc. Chem. Res.* **2014**, *47*, 3301–3309.
33. Kemp, N. T.; Kaiser, A. B.; Trodahl, H. J.; Chapman, B.; Buckley, R. G.; Partridge, A. C.; Foot, P. J. S. Effect of Ammonia on the Temperature-Dependent Conductivity and Thermopower of Polypyrrole. *J. Polym. Sci. B Polym. Phys.* **2006**, *44*, 1331–1338.
34. Krishnaswamy, S.; Ragupathi, V.; Raman, S.; Panigrahi, P.; Nagarajan, G. S. Optical Properties of P-Type Polypyrrole Thin Film Synthesized by Pulse Laser Deposition Technique: Hole Transport Layer in Electroluminescence Devices. *Optik* **2019**, *194*, 163034.
35. Li, M.; Luo, C.; Zhang, J.; Yang, J.; Xu, J.; Yao, W.; Tan, R.; Duan, X.; Jiang, F. Electrochemical Doping Tuning of Flexible Polypyrrole Film with Enhanced Thermoelectric Performance. *Surf. Interfaces* **2020**, *21*, 100759.
36. Matsuura, Y.; Taniguchi, I. Single-Molecule Tunnel Magnetoresistance of p-Type Doped Polypyrrole. *Org. Electron.* **2019**, *69*, 114–119.
37. Kaiser, A. B. Systematic Conductivity Behavior in Conducting Polymers: Effects of Heterogeneous Disorder. *Adv. Mater.* **2001**, *13*, 12–13.
38. Kang, W.; Jérôme, D.; Valade, L.; Cassoux, P. Thermopower Measurement of the Organic Condctor TTF[Ni(dmit)₂]₂ at Ambient Pressure. *Synth. Met.* **1991**, *41–43*, 2343–2345.
39. Wang, Y.; Liu, G.; Sheng, M.; Yu, C.; Deng, Y. Flexible Thermopower Generation over Broad Temperature Range by PANI/Nanorod Hybrid-Based p-n Couples. *J. Mater. Chem. A* **2019**, *7*, 1718–1724.